A solvent-exposed cysteine forms a peculiar Ni(II)-binding site in the metallochaperone CooT from Rhodospirillum rubrum.

Marila Alfano, Giulia Veronesi, Francesco Musiani, Barbara Zambelli, Luca Signor, Olivier Proux, Mauro Rovezzi, Stefano Ciurli, Christine Cavazza

RESEARCH ARTICLE

A solvent-exposed cysteine forms a peculiar Ni(II)-binding site in the metallochaperone CooT from *Rhodospirillum rubrum*

Marila Alfano,[a] Giulia Veronesi,[a] Francesco Musiani,[b] Barbara Zambelli,[b] L. Signor,[c] O. Proux,[d] M. Rovezzi,[d] Stefano Ciurli,*[b] Christine Cavazza *[a]

Abstract: In *Rhodospirillum rubrum*, the maturation of carbon monoxide dehydrogenase (CODH) requires three nickel chaperones, namely *Rr*CooC, *Rr*CooT and *Rr*CooJ. Recently, the biophysical characterization of R*r*CooT homodimer and the X-ray structure of its apo-form revealed the existence of a solvent exposed Ni(II)-binding site at the dimer interface, involving the strictly conserved Cys2. Here, a multifaceted approach that used NMR and X-ray absorption spectroscopies, complemented with structural bio-modelling methodologies, was used to characterise the binding mode of Ni(II) in *Rr*CooT. This study suggests that Ni(II) adopts a square-planar geometry via a N_2S_2 coordinating environment that comprises the two thiolate and amidate groups of both Cys2 residues at the dimer interface. The existence of a diamagnetic mononuclear Ni(II) centre with bis-amidate/bis-thiolate ligands, coordinated by a single cysteine motif, is unprecedented in biology and raises the question of its role in the activation of CODH, at the molecular level.

Introduction

Despite their low occurrence in nature, the importance of Ni-dependent enzymes in Archaea, bacteria, fungi, algae and higher plants has been widely recognized in the last few decades. These enzymes use a Ni-containing active site to catalyse essential reactions such as the reduction of anionic superoxide radical, [1] urea hydrolysis, [2] methane production, [3] or H_2/CO reversible oxidation. [4] In the hydrogenogenic carboxydotroph *Rhodospirillum rubrum*, the nickel-dependent carbon monoxide dehydrogenase (*Rr*CODH) is a key enzyme in the energy metabolism.[5] Indeed, a characteristic feature of this versatile photosynthetic bacterium is its capacity to use CO as the sole energy source under anaerobic conditions, via the water-gas shift reaction ($H_2O + CO \rightarrow CO_2 + H_2$). [6] In this reaction, *Rr*CODH plays a central role by catalysing the oxidation of CO to CO_2, coupled to the H_2 production catalysed by an energy-converting [NiFe]-hydrogenase. [7] *Rr*CODH is a homodimer bridged by an intermolecular [4Fe-4S]-cluster (D-cluster), with each monomer containing a [4Fe-4S]-cluster (B-cluster) and a peculiar [Ni-4Fe-4S] active site (C-cluster). [8] The CO oxidation occurs at the C-cluster, whereas the B-clusters are involved in the electron transfer between the active site and its physiological partner, the ferredoxin CooF. [9] Nickel insertion into the active site is the essential step for the enzyme activation: Ni-deficient CODH, produced in nickel-depleted growth media, presents a fully assembled $[Fe_4S_4]$ C-cluster that can be partially reactivated *in vitro* by Ni(II) addition under reductive conditions. [10]

A common feature of metalloenzymes is the requirement of auxiliary proteins, typically involved in the metallo-centre biosynthesis and assembly. [11] In the case of *Rr*CODH, the *cooFSCTJ* operon contains the *cooCTJ* genes encoding three different nickel-binding proteins, CooC, CooT and CooJ, present downstream the structural *cooS* gene that encodes CODH. [12]

[a] University of Grenoble Alpes, CEA, CNRS, IRIG, CBM, F-38000 Grenoble, France
[b] Laboratory of Bioinorganic Chemistry, Department of Pharmacy and Biotechnology, University of Bologna, Via Giuseppe Fanin 40, I-40127 Bologna (Italy)
[c] University of Grenoble Alpes, CEA, CNRS, IRIG, IBS, F-38000 Grenoble, France.
[d] Univ. Grenoble Alpes, CNRS, IRD, Irstea, Météo France, OSUG, FAME, 38000 Grenoble, France

*Rr*CooC is Ni-dependent ATPase, proposed to provide the energy required for the maturation process and able to dimerize by binding Ni(II) via a CXC motif that is conserved among CooC homologs. [13] *Rr*CooJ is a 25-kDa homodimeric protein containing two distinct metal-binding sites: a C-terminal histidine tail composed by sixteen histidines and two cysteines able to bind four Ni(II) per dimer, and a strictly conserved HX_3HX_3H binding site present in the N-terminal region and binding one Ni(II) per dimer. [14] Finally, *Rr*CooT is a small homodimeric protein of 66 residues able to bind one Ni(II) per dimer with a dissociation constant in the nanomolar range, using Cys2. [15] Looking at the amino acid recurrence in proteins, cysteine is one of the least abundant residues. [16] However, when present, cysteines are required in essential functional sites, such as structural disulphide bridges, iron-sulphur cluster coordination or sulphur-rich metal coordination sites in metalloproteins. [16] Based on the analysis of protein structure databases, this residue shows the characteristic feature of being either highly conserved in buried cysteine clusters, or poorly conserved when isolated and located at the protein surface. [16] In *Rr*CooT, Cys2 is the only cysteine in the protein sequence and the crystal structure of the apo-protein revealed its solvent exposure. [15] Unexpectedly, while the amino acid sequences of the 111 CooT homologues identified in anaerobic archaea and bacteria show a remarkable large variability, Cys2 is the only strictly conserved residue, [15] in this way violating the general conservation vs. structure pattern. Thus, the evolutionary conservation of the solvent-exposed cysteine in CooT proteins suggests its importance to meet a specific and essential functional role.

By analogy, several well-described nickel proteins possess Ni-binding sites containing multiple cysteine residues in the proximity of the N-terminus. They form the well-known Ni-hook motif "HCX_2PCGXY" in the nickel-dependent superoxide dismutase (NiSOD) [17] or the high-affinity "MCX_2CXC" site in HypB, [18] a GTPase involved in [Ni-Fe]-hydrogenase for which the Ni(II)-binding mode is not definitively established. The particularity of *Rr*CooT is the presence of a Ni-binding site in the N-terminal region, with a single cysteine motif, raising the question of its metal-coordination mode. The X-ray structure of apo-*Rr*CooT revealed that its dimerization brings the two $Cys2_A$ and $Cys2_B$ residues (belonging to the two monomers A and B) in close proximity, likely triggering the formation of a Ni-binding site. Indeed, mutation of Cys2 to Ser obliterated Ni(II)-binding to CooT, revealing the essential role of the Cys-thiolate groups. [15] However, no structural information is yet available for the Ni-binding site in *Rr*CooT.

In the present study we investigated the structural details of the Ni(II)-binding site of *Rr*CooT using a multifaceted approach that involved NMR and X-ray absorption spectroscopies complemented with structural bio-modelling methodologies. The results support the presence of an unprecedented metal-binding motif that involves a pair of isolated solvent exposed cysteine bound to a square-planar Ni(II) ion in a N_2S_2 coordination environment, with a *bis*-thiolate/*bis*-amidate ligation in a *trans* configuration.

Results

Metal-binding motifs in the CooT family

Alignment of 91 non-redundant CooT sequences revealed the existence of two distinct nickel-binding motifs in the CooT family: the “Cys2-His55” motif, previously characterized in the putative CooT from *Carboxydothermus hydrogenoformans* (*Ch*CooT),[19] is conserved in 64 CooT homologues (corresponding to 70.3% of all sequences) (Figure S1). It is mainly found in bacteria (48 sequences) and in some Archaea (16 sequences). On the other hand, the “Cys2” motif is found in 16 archaeal and 7 bacterial CooT sequences (25.3 % of all sequences) (Figure 1A). In addition, in three methanogens, a second cysteine is also found in position 4, forming a putative not characterized “Cys2-Cys4” motif. *Rr*CooT belongs to the “Cys2” motif group, as shown in Figure 1A.

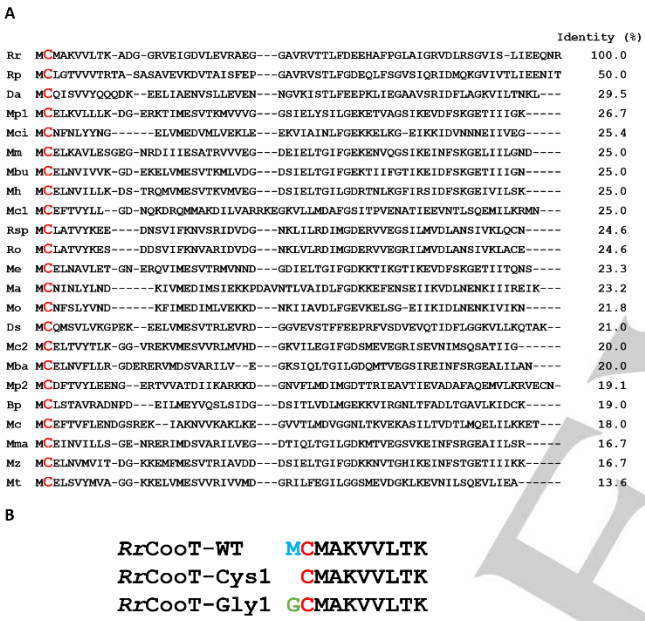

Figure 1. (**A**) Sequence alignment of CooT homologues possessing the “Cys2” motif. Cys2 is in red. Rr: *Rhodospirillum rubrum* ATCC11170, Da: *Desulfurivibrio alkaliphilus* AHT2, Ro: *Ruminococcus obeum* A2-162, Mp1: *Methanolobus psychrophilus*1 R15; Mh: *Methanomethylovorans hollandica* DSM 15978, Mci: *Methanocaldococcus infernus* ME, Me: *Methanohalobium evestigatum* Z-7303, Mm: *Methanohalophilus mahii* DSM 5219, Ma: *Methanococcus aeolicus* Nankai-3, Mc2: *Methanosaeta concilii2 GP6, Rsp:* Ruminococcus sp, Mbu: *Methanococcoides burtonii* DSM 6242, Mo: *Methanothermococcus okinawensis* IH1, Mc1: *Methanosaeta concilii1* GP6, Ds: *Desulfocapsa sulfexigens* DSM 10523, Mc: *Methanocella conradii* HZ254, Mp2: *Methanolobus psychrophilus*2 R15, Bp: *Butyrivibrio proteoclasticus* B316, Mz: *Methanosalsum zhilinae* DSM 4017, Mba: *Methanosarcina barkeri* MS, Mma: *Methanosarcina-mazei* S-6, Mt: *Methanosaeta thermophila* PT, Rp: *Rhodopseudomonas palustris* BisB18. Identity percent corresponds to the conserved amino acids between each sequence and *Rr*CooT sequence. (**B**) N-terminal sequences of *Rr*CooT-WT, *Rr*CooT-Cys1 and *Rr*CooT-Gly1.

Modification of the N-terminus of *Rr*CooT and Ni(II) binding

The thiolate groups of $Cys2_A$ and $Cys2_B$ provide two potential coordinating ligands for Ni(II). However, at least two additional ligands are required to complete the coordination environment of Ni(II) in a square-based, tetrahedral or octahedral geometry. Considering the position of the metal-binding site at the beginning of the protein sequence, the N-terminal amino group would be a logical choice as a Ni donor ligand. However, in all identified sequences shown in Figure 1A the first residue is a methionine, which is often processed by methionine amino peptidases (MetAP), thus raising the question as to whether this residue is strictly necessary to complement the thiolate groups of Cys2 for Ni binding. No information is available about the processing of Met1 in *Rr*CooT by MetAP in *R. rubrum*. Therefore, in order to understand the role of Met1 and the impact of the position of the conserved Cys residue in the sequence at the N-terminus, different variants were constructed. Overproduction of *Rr*CooT in *E. coli* grown for 16 h in a minimal medium at 25 °C led to a major Met1-containing form (about 80% of the total protein, as previously described in [15]), corresponding to *Rr*CooT-WT (Figure 1B). On the other hand, replacement of the minimal medium with a rich-growth medium, raising the temperature to 37 °C and using an induction time of 4 h resulted in a form of *Rr*CooT lacking Met1 (*Rr*CooT-Cys1), (Figure 1B). The latter protocol was also used to express a synthetic gene featuring a Gly residue inserted between Met1 and Cys2, producing the *Rr*CooT-Gly1 variant also lacking the Met residue at the N-terminus (Figure 1B). The identity of these two protein variants was confirmed by ESI-MS (Figure S2). The ESI-MS spectrum of *Rr*CooT-Gly1 showed the expected single peak at 7,022.11 Da, confirming the identity and homogeneity of this mutant.

Considering that N-terminal cysteines are known to be highly reactive,[20] the integrity of the thiol groups in *Rr*CooT-Cys1 was tested after removal of the reducing agent TCEP and overnight exposure to air. In the case of *Rr*CooT-Gly1, this treatment led to the appearance of a major species, with a mass of 14,042.24 Da, corresponding to a homodimer induced by the formation of a disulphide bridge between $Cys2_A$ and $Cys2_B$ with the loss of 2 Da, due to the oxidation of the two thiol groups (Figure S2). On the contrary, ESI-MS of several samples of *Rr*CooT-Cys1 revealed a mixture of two species: the first, at 6,964.93 Da, corresponds to the Met1-processed monomer, while the second showed an unknown adduct of 26 Da. This adduct is never observed when the Met1 is present at the N-terminus of *Rr*CooT. Moreover, the amount of the second species varied from 50 to 90% depending on the *Rr*CooT-Cys1 samples. The 26 Da-mass is consistent with the formation of a S-CN moiety on Cys2 [21] and ESI-MS experiments showed that its presence hinders the formation of the disulphide bridge (Figure S2), suggesting that Met1 processing drastically affects the thiol group reactivity.

Biophysical characterization of *Rr*CooT-Cys1 and *Rr*CooT-Gly1

The Ni(II) binding ability of the different constructs was estimated using UV/vis and circular dichroism (CD) spectroscopy in the near-UV/vis range (250-700 nm) and by isothermal titration calorimetry (ITC). UV/vis and CD spectra were recorded under anaerobic conditions to prevent the formation of disulphide bridges, while ITC titrations were conducted in the presence of the reducing agent TCEP. In the UV/vis spectra of *Rr*CooT-WT and *Rr*CooT-Gly1, transition bands at 345 nm, 427 nm, 475 nm and 530 nm were observed (Figure 2A, B). Similar UV/vis signatures have been previously observed for square planar Ni(II) coordinated to di-amido/di-thiolato ligands in Ni-containing superoxide dismutase (NiSOD) model peptides [22] and a NiSOD mutant, in which the amidate/amine coordination was switched to a bis-amidate mode by adding an alanine residue to the N-terminus. [23] The CD spectrum of *Rr*CooT-Gly1 (Figure 2C) is similar to the previously published spectrum of *Rr*CooT-WT, [15] with ligand-to-metal charge transfer and d-d transitions at 260 nm (-), 287 nm (+), 310 nm (+), 355 nm (+), ~410 nm (-) and 475 nm (-). The presence of CD bands between 400 and 600 nm suggests the presence of a Ni(II)-bound amide, rather than amine, nitrogen binding, as previously observed for Ni(II)-containing peptides mimicking NiSOD. [24]

A calorimetric Ni(II) titration of *Rr*CooT-Gly1 showed negative peaks following Ni(II) injections, indicative of exothermic events (Figure 2D). The shape of the binding isotherm obtained from data integration indicated the occurrence of two independent binding events. The first event involves the binding of one Ni(II) ion to the protein dimer with a high affinity (K_{A1} = 3 ± 1 x 10^7; K_{D1} = 50 ± 20 nM, ΔH_1 = -9.6 ± 0.3 kcal mol^{-1}; ΔS_1 = +2.10 kcal mol^{-1} K^{-1}), while the second binding event shows a lower affinity (K_{A2} = 3 ± 2 x 10^5; K_{D2} = 3 ± 0.6 µM, ΔH_2 = -4.8 ± 0.7 kcal mol^{-1}, ΔS_2 = +13.2 kcal mol^{-1} K^{-1}). These data are similar to those previously obtained for *Rr*CooT-WT,[15] indicating that *Rr*CooT-Gly1 contains a preserved high affinity Ni(II) binding site, as well as an additional weaker metal site, most likely non-physiological. The similar metal binding behaviour of *Rr*CooT-Gly1 and *Rr*CooT-WT indicates that the nature of the side chain on the first residue of the sequence does not influence the Ni(II) binding properties of the high affinity site of *Rr*CooT. On the other hand, the *Rr*CooT-Cys1 mutant spectrum does not show any CD signal upon Ni(II) addition, indicating the absence of Ni(II) binding (Figure 2C). This was confirmed by ITC, which showed that the binding event is fully abrogated (Figure 2D). These observations indicate that the position of the conserved Cys as the second residue in the sequence of *Rr*CooT is essential for binding, and consequently that Met1 processing by MetAP is most likely not occurring in *R. rubrum.*

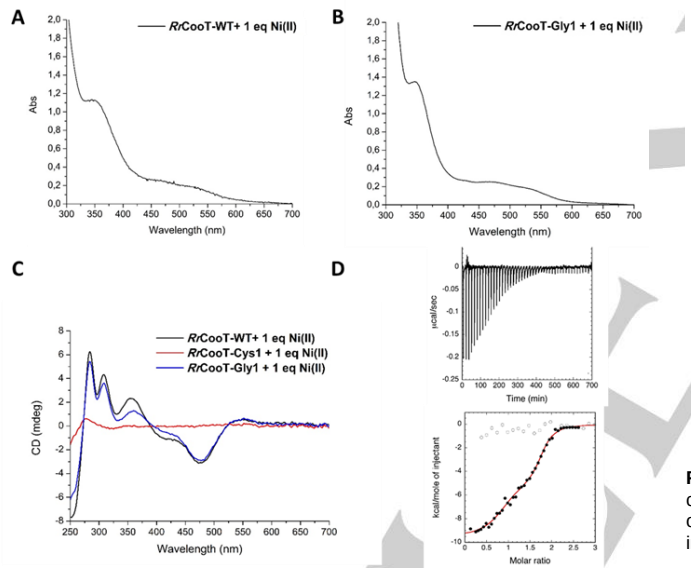

Figure 2: (**A**) UV/vis spectrum of *Rr*CooT-WT (500 µM dimer) in the presence of one equivalent of Ni(II), in 50 mM HEPES buffer at pH 7.5, under anaerobic conditions; ε_{345} = 2254 M^{-1} cm^{-1}, ε_{475} = 502 M^{-1} cm^{-1} and ε_{530} = 345 M^{-1} cm^{-1}. (**B**) UV/vis spectrum of *Rr*CooT-Gly1 (630 µM dimer) in the presence of one equivalent of Ni(II), in 50 mM HEPES buffer at pH 7.5; ε_{345} = 2134 M^{-1} cm^{-1}, ε_{427} = 417 M^{-1} cm^{-1}, ε_{475} = 396 M^{-1} cm^{-1}, andε_{530} = 279 M^{-1} cm^{-1}. (**C**) CD spectra for *Rr*CooT-WT (black line), *Rr*CooT-Cys1 (red line) and *Rr*CooT-Gly1 (blue line) registred for a 25µM dimer concentration in the presence of one molar equivalent of Ni(II). (**D**) Top panel: representative raw plot of the ITC data of Ni(II) (240 µM) injected onto the *Rr*CooT-Gly1 solution (12 µM); bottom panel: integrated heat data as a function of the metal-to-protein molar ratio for *Rr*CooT-Gly1 (filled circles) and *Rr*CooT-Cys1 (hollow circles). The continuous line represents the best fit obtained for *Rr*CooT-Gly1 titration, using a model involving two independent sets of binding sites for Ni(II), as described in the text.

The thiol modification appears to be the most likely reason for *Rr*CooT-Cys1 being unable to bind Ni(II). However, the removal of the Met1 also changed the amide group of Cys2 to a protonated N-terminal amine, which could also impact Ni(II) binding. To go further into the characterization of the Ni-binding site of *Rr*CooT-WT and the identification of the N donor ligands, NMR spectroscopy experiments were carried out on the apo- and holo-forms of the protein.

Assignment of the NMR spectra of apo-*Rr*CooT-WT

Heteronuclear 2D and 3D NMR spectra of dimeric *Rr*CooT-WT were recorded and analysed, and backbone assignments were obtained using the scalar connectivities provided by triple resonance experiments (Table S1). The assigned ^{1}H,^{15}N HSQC spectrum recorded at 950 MHz ^{1}H Larmor frequency is shown in Figure 3. The large spectral dispersion of the signals in the ^{1}H dimension unambiguously indicates that the protein is well-folded in solution, while the number of cross-peaks is consistent with the number of residues in a single subunit, supporting a symmetrical average orientation of the two monomers. The identification of amide ^{1}H and ^{15}N peaks was obtained at 950 MHz for 63 out of the 66 residues following a standard sequential assignment procedure (Table S2).

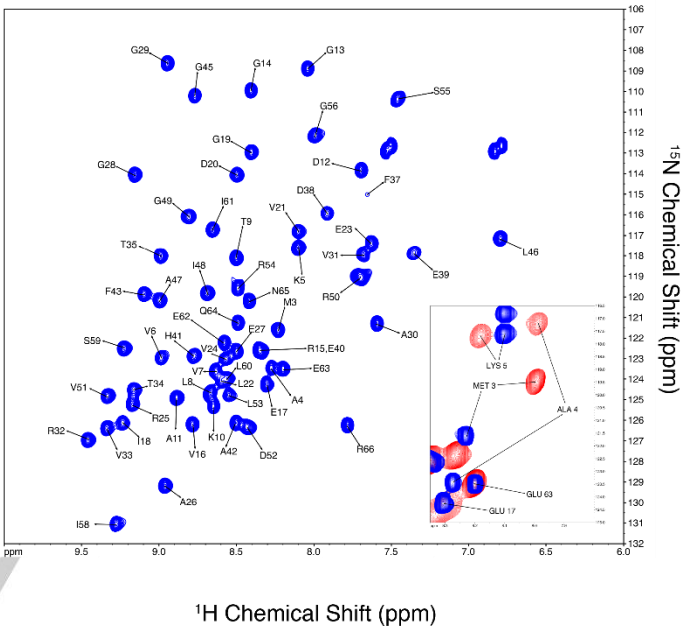

Figure 3. ^{1}H,^{15}N HSQC spectrum of *Rr*CooT-WT at 950 MHz with the corresponding assignment. The inset shows the overlay between the spectrum of apo-*Rr*CooT-WT (blue) at 950 MHz and holo-*Rr*CooT-WT (red) at 500 MHz in the region covering the N-terminus residues.

The Pro44 residue is not observable in the ^{1}H,^{15}N HSQC spectrum because it does not have the peptide NH group, while the N-terminal Met1 is not observable because of fast proton exchange with water of its NH_3^+ terminal group with water. The peptide NH signal for the remaining Cys2 residue was also not observable in the spectrum at 950 MHz probably because its NMR signal is broadened beyond detection due to conformational exchange phenomena occurring with rates comparable to the frequency differences among the different conformers. Attempts to observe its signal in ^{1}H,^{15}N HSQC spectra taken at 500 MHz were also unsuccessful, indicating that Cys2, and presumably even more so Met1, undergoes conformational changes with correlation times in the sub-microseconds time scale. On the other hand, the peaks corresponding to Met3 and Ala4, while visible at 950 MHz, also disappeared in the spectra taken at 500 MHz, consistently with a progressively slower conformation exchange rate for residues gradually farther away from the N-terminus. Additional attempts to observe the peaks corresponding to Met1 and Cys2 in the ^{1}H,^{15}N HSQC spectra, carried out by lowering or raising the temperature at all tested fields, were

unsuccessful. However, the Cα/Hα and Cß/Hß pairs of Cys2 were observed in the spectra of apo-*Rr*CooT-WT using HNCO/HN(CA)CO and HNCACB/CBCA(CO)NH triple resonance spectra (Table S1).

The program TALOS+ [25] was used to correct the referencing for Hα, Cα, Cß, and CO chemical shifts, through an empirical correlation.[26] Then, the HN, N, Hα, Cα, Cβ, and CO, chemical shifts assigned to the residues of apo-*Rr*CooT-WT were used by TALOS+ to estimate the φ and ψ backbone torsion angles and the consequent secondary structure (Figure 4) using an artificial neural network. [25] A negative TALOS+ score indicates a propensity for α-structure or loop, while a positive TALOS+ score indicates a propensity for β-structure. Figure 4 shows the good agreement between the secondary structure determined by NMR in solution and that obtained by solid-state crystallography of the apo-protein,[15] demonstrating the conservation of the protein structure independently of its solid or solution state.

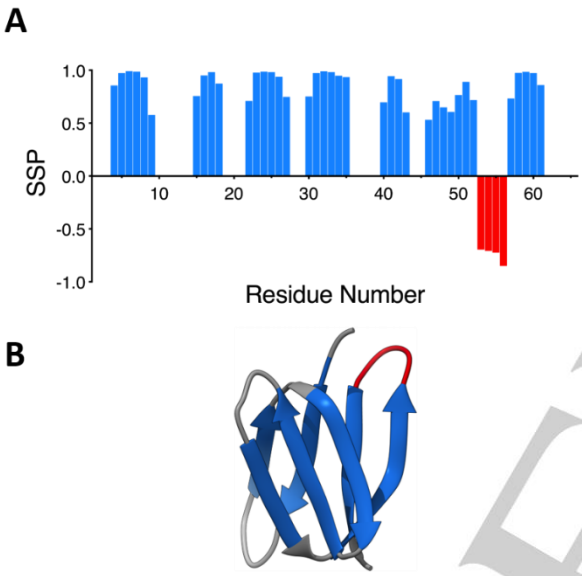

Figure 4. (**A**) Artificial neural network predicted secondary structure (SSP) for apo-*Rr*CooT-WT, using Hα, N, Cα and Cβ backbone secondary NMR chemical shifts obtained at 950 MHz. The blue and red bars indicate beta and helix/loop secondary structure, respectively. (**B**) The ribbon scheme of the crystal structure of the apo-*Rr*CooT monomer (PDB id: 5N76) is shown colored according to the TALOS+ predicted secondary structure to highlight the consistency between the solution NMR and the solid-state crystallographic data.

Assignment of the NMR spectra of holo-*Rr*CooT-WT

The analysis of the modifications occurring in the $^{1}H,^{15}N$ HSQC spectrum of apo-*Rr*CooT-WT at 500 MHz and 950 MHz by subsequent addition of 0.0, 0.5, 1.0 and 2.0 equivalents of Ni(II) per protein dimer revealed that the chemical shift and intensity of most $^{1}H/^{15}N$ backbone amide cross-peaks were largely unperturbed, and that only few residues were affected by significant chemical shift changes in the slow exchange limit. No modification was observed between the 1.0 and 2.0 titration steps, confirming the stoichiometry of 1 Ni(II) per *Rr*CooT-WT dimer determined by ITC for the high-affinity site. The lack of signal disappearance upon Ni(II) addition indicates that the metal ion is diamagnetic in holo-*Rr*CooT-WT. The marginally affected cross-peaks were assigned in the Ni(II)-bound *Rr*CooT-WT on the basis of a simple closest-neighbour matching approach. The analysis of the HNCACB/CBCA(CO)NH pair of triple resonance experiments at 500 MHz confirmed this initial assignment and further extended it to comprise all observable signals in the $^{1}H,^{15}N$ HSQC spectrum of holo-*Rr*CooT-WT, with the exception of Met1 and Cys2. Significantly, the signals corresponding to Met3 and Ala4, not observable in the 500 MHz spectrum of apo-*Rr*CooT-WT, became visible again at this magnetic field upon Ni(II) addition. This observation implicates the hypothesis that Ni(II) binding occurring at the N-terminal region of the protein, causes a significant decrease of its mobility. Finally, the very large chemical shifts induced by Ni(II) binding on Cys2 Cα (from 55.55 ppm to 61.99 ppm) and Cß (from 25.56 to 35.59 ppm), and the very small chemical shifts induced on Met3 Cα (from 52.23 ppm to 52.36 ppm) and Cß (from 31.31 to 31.12 ppm) reveal that Cys2 is part of the metal coordination environment, and that the protein structure is negligibly affected by nickel binding beyond this residue. The Ni(II)-induced chemical shift perturbation (CSP), mapped on the protein surface (Figure 5) confirmed that the region of *Rr*CooT at or near the N-terminal residues is involved in Ni(II) binding, with the thiol group of Cys2 being the most likely candidate for direct metal ion coordination.

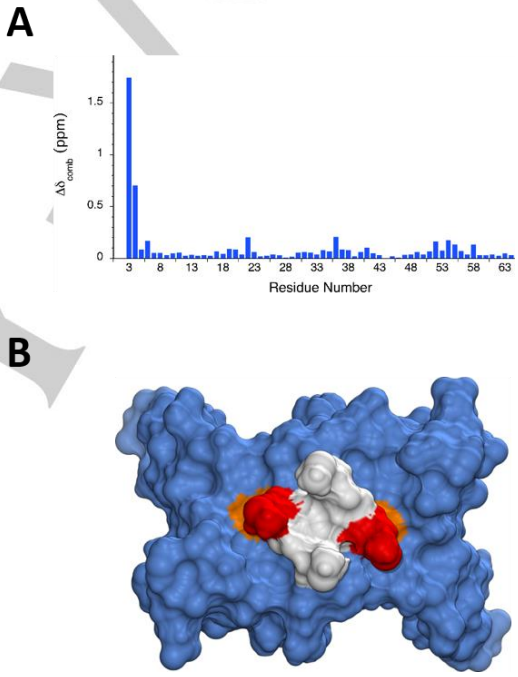

Figure 5. (**A**) Plot of combined chemical shift perturbation $\Delta\delta_{comb}$ upon Ni(II) binding to apo-*Rr*CooT-WT, along the protein sequence. (**B**) The protein surface, calculated from the X-ray structure of apo-*Rr*CooT and color-coded according to the size of $\Delta\delta_{comb}$ ($\Delta\delta_{comb}$ > 1.0 red; 0.5 < $\Delta\delta_{comb}$ < 1.0 orange; $\Delta\delta_{comb}$ < 0.5 blue; non-assigned residues M1 and C2 are shown in white).

This hypothesis was confirmed by the observation that no perturbation in the $^{1}H,^{15}N$ HSQC spectrum was induced by addition of Ni(II) to a sample of apo-*Rr*CooT-WT stored for several days in air, a treatment shown by ESI-MS to cause oxidation of the two Cys2 residues in the dimer (see above), while the typical spectrum of holo-*Rr*CooT-WT was re-established upon addition of TCEP, known to reduce disulphide bonds. These NMR spectroscopic results indicate that Ni(II) binding in *Rr*CooT involves the thiolate groups of the two Cys2 residues, yielding a square-planar or square-pyramidal geometry for a diamagnetic Ni(II) ion in holo-*Rr*CooT-WT. In order to further examine the coordination environment of the Ni(II) site, X-ray absorption spectroscopy was applied.

Preliminary X-ray absorption spectroscopy analysis

Ni K-edge X-ray absorption spectra of *Rr*CooT-WT in complex with 0.9 Ni(II) molar equivalent per dimer (Ni-*Rr*CooT) were acquired under cryogenic conditions. The X-ray Absorption Near Edge Structure (XANES) spectrum of the holo-protein is shown in Figure 6A, in which a weak pre-edge peak at ~ 8332 eV associated to 1s → 3d electronic transitions, and a resolved maximum at ~8338 eV, are observed. The latter is associated to 1s → $4p_z$ transitions and has been shown to be indicative of square planar Ni coordination geometry. [27]

For comparison with Ni-*Rr*CooT, we measured the spectra of two Ni(II) tetra-coordinated square planar compounds exhibiting different ligand environments (Figure S3) [28] (Figure 6): both N_2S_2 and S_4 coordination models give rise to a resolved peak at ~8338 eV as reported in literature, and a 1s → 3d feature of comparable intensity with respect to that observed for Ni-*Rr*CooT. The area of Gaussian peaks reproducing the 1s → 3d transition, which provides information on the coordination geometry at the Ni site, was calculated for protein and reference samples.

The best-fitting curve for Ni-*Rr*CooT is reported in the inset of Figure 6A, and the estimated curve parameters in Table S4. The peak areas fall in the range previously described for a collection of four-coordinate, square planar Ni compounds (area < $2.9 \cdot 10^{-2}$ eV), and differ dramatically from the areas calculated for tetrahedral and five-coordinated Ni complexes (area > $4.2 \cdot 10^{-2}$ eV). [41] This analysis, together with the observed resolved 1s → $4p_z$ transition, strongly supports a square planar Ni binding geometry in Ni-*Rr*CooT, consistently with NMR spectroscopy.

In order to disclose the nature of the Ni ligands in the *Rr*CooT dimer, the first shell peak of the Fourier-transformed EXAFS signal was analysed in the range R = 1.0 - 2.2 Å. Considering the results obtained from the biophysical and spectroscopic characterization of the holo-protein described in previous sections, we expect the Ni-binding atoms to belong to the amino acids in position 1 and 2. Therefore, coordination spheres composed of S and N atoms were considered, given that these atoms can be provided either by the thiolate side chain of Cys2 or by the protein backbone, respectively. Four ligands in planar geometry were considered according to the XANES analysis. The first-shell peak is best fitted by a N_2S_2 coordination (Figure 6B), whereas a N-only coordination fails to reproduce the experimental spectra. The N_2S_2 coordination is also suggested by the similarity in the EXAFS oscillations between the experimental spectrum of Ni-*Rr*CooT and of the N_2S_2 reference compound (Figure 6A**,** dotted lines). Remarkably, two distinct Ni-N distances had to be considered, whereas if a common distance was assigned to both Ni-N scattering paths, the first peak of the FT EXAFS spectrum could not be reproduced. Removing the degeneracy in the Ni-N distances resulted in a net improvement of the agreement between fit and experimental data (R-factor drops from 4.9% to 0.6%), and to the determination of first-shell Debye-Waller factors that were fitted to unphysical values in case of degenerated Ni-N distances (see Table 1, fit number 1 vs 2). In order to obtain reliable structural models for ab initio EXAFS refinement, a well-established computational approach was adopted. [29]

Modelling of the *Rr*CooT high affinity Ni(II)-binding site

Two sets of models were generated by considering all the possible configurations for a square planar Ni(II) geometry (Scheme 1). In the first set of models, the Ni(II) Met1 terminal amine N atom and the Cys2 thiolate S atom from each monomer were considered (models Amino-Cis1, Amino-Cis2 and Amino-Trans hereafter). In the second set, the backbone N atom of Cys2 from each monomer was instead examined (models Amide-Cis1, Amide-Cis2 and Amide-Trans hereafter). Initial distances were taken from the fit of the first-shell peak of the Fourier-Transformed EXAFS signal (Table 1). The constraints used in the modelling stages are reported in Table S5 and Table S6).

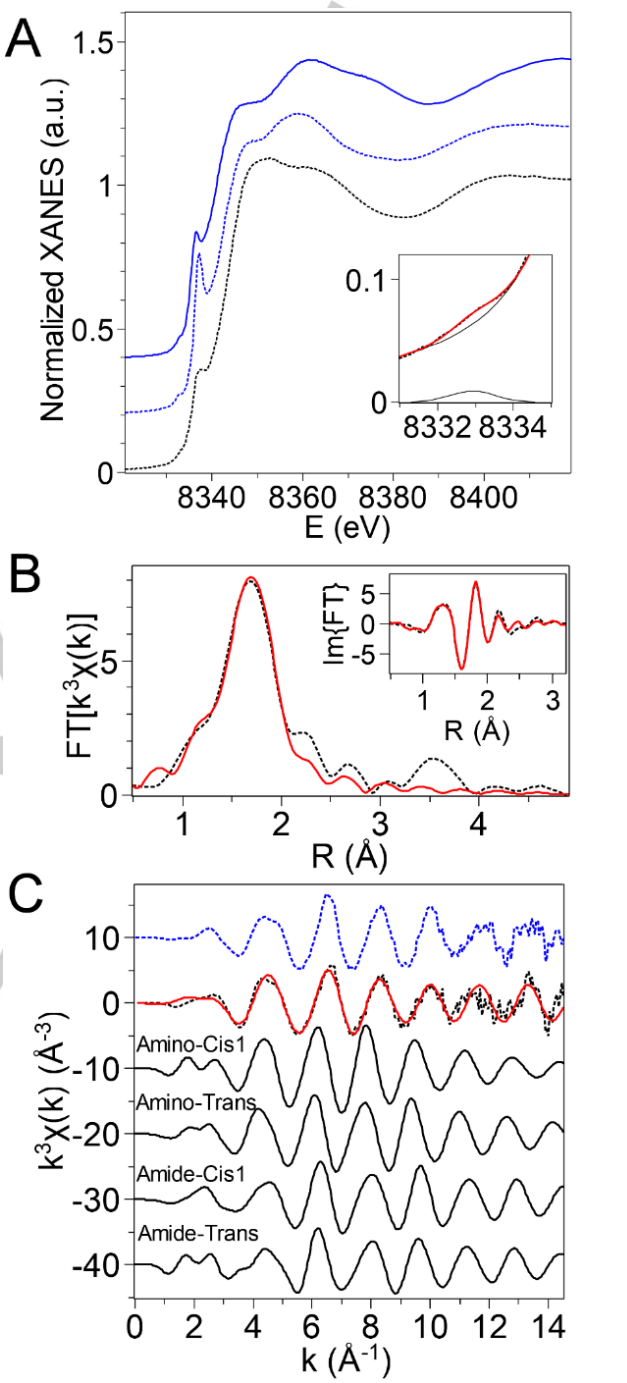

Figure 6 (**A**) Ni K-edge XANES spectra of square-planar Ni(II) reference compounds (blue) with N_2S_2 (dotted line) and S_4 (solid line) coordination, and of Ni-*Rr*CooT (black dots). Inset: magnification of the 1s → 3d transition energy region and fit (red) of the experimental data (black dots). The two components of the fitting curve are represented as black solid lines. (**B**) Fourier Transformed experimental EXAFS spectrum of Ni-*Rr*CooT (black dotted line) and theoretical curve providing the best fit to the first shell peak (red solid curve). The imaginary part of both curves is reported in the inset. (**C**) k^3-weighted experimental EXAFS spectra of Ni-*Rr*CooT (black dashed line) and of a Ni(II)N_2S_2 reference compound (blue dashes). Theoretical spectra (black solid lines) generated from optimized structures of Ni-CooT varying the N donor (amine N of Met1 or amide N of Cys2) and the relative arrangements of first-shell ligands (S atoms in trans or cis position). Best fitting curve (red solid line) for the experimental data starting from the optimized model "amide-trans".

Scheme 1

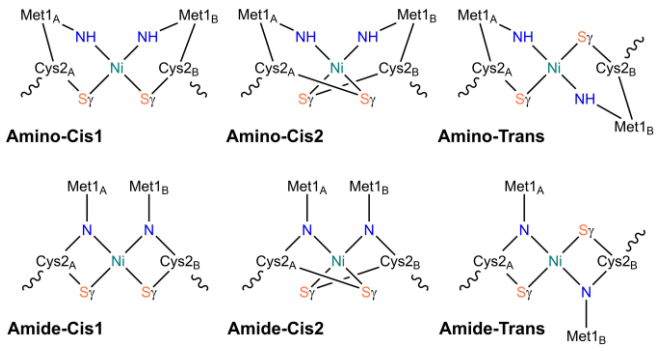

Table 1. Structural and dynamic parameters of the Ni-*Rr*CooT site, extracted from *ab initio* fitting of Ni K-edge EXAFS data based on different models (see text). The 1σ standard deviation error relative to the last digit is reported in parentheses

Fit number	Ni-neighbours	R (Å)	σ^2 (10^{-3} Å^2)	ΔE_0 (eV)	R-factor (%)
1	2N	2.07 (4)	50 (10)	-10 (2)	4.9
	2S	2.13 (3)	3 (2)		
2	N	1.87 (4)	2 (2)	-8.2	0.6
	N	2.09 (4)	2 (2)	(5)	
	2S	2.14 (1)	3.0 (6)		
3	N	1.86 (2)	2.0 (10)	-9.4 (8)	5.9
	N	2.10 (2)	2.0 (10)		
	2S	2.14 (1)	2.7 (6)		
	6C*	2.90-3.37	7 (5)		

In all calculated models, the Ni(II) ion binds at the dimer interface that connects the N-terminal portion of each monomer (Figures S4 and S5). The details of the metal binding regions resulting from the modelling are reported in Figure 7. The Amino-Cis1 model (Figure 7A) resulted in a Ni(II) ion in a nearly ideal square planar coordination geometry [root mean square deviation from the ideal geometry (rmsd_ig) = 0.029 Å]. The plane formed by the nickel ligands is perpendicular to the *Rr*CooT dimerization interface, while the metal binding site is fully exposed to the solvent. In the Amino-Cis2 model (Figure 7B), the orientation of the metal binding region appears to be similar to that in the Amino-Cis1 model, but the Ni(II) coordination geometry is strongly distorted (rmsd_ig = 0.768 Å). Finally, the Amino-Trans model (Figure 7C) resulted again in nearly ideal square planar metal coordination geometry (rmsd_ig = 0.040 Å), and a different disposition of the plane formed by the nickel ion and the four ligands. Indeed, in the Amino-Trans model the plane formed by the Ni ligands is parallel to the dimer's major axis and the Ni(II) ion is exposed to the solvent only on one side. In both Amino-Cis1 and Amino-Cis2 models, the side chains of both $Met1_A$ and $Met1_B$ are buried inside the protein, while in the case of model Amino-Trans model, the Met1 side chain from both monomers is exposed to the solvent. The Amide-Cis1 model (Figure 7D) resulted in a slightly distorted square planar metal coordination geometry (rmsd_ig = 0.192 Å). As in all previous Cis models, the plane formed by the nickel ion and its ligands is perpendicular to the *Rr*CooT dimerization interface and the metal binding site is fully exposed to the solvent. Also, in the case of the Amide-Cis2 model (Figure 7E), the metal-

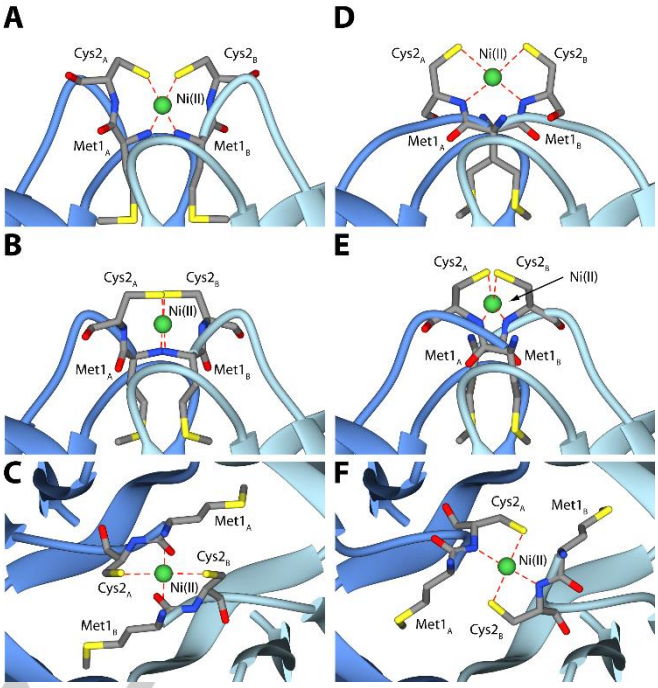

Figure 7. Detail of the modelled Ni(II) binding site of *Rr*Coot in the case of model Amino-Cis1 (**A**), Amino-Cis2 (**B**), Amino-Trans (**C**), Amide-Cis1 (**D**), Amide-Cis2 (**E**), and Amide-Trans (**F**) (see Scheme 1). The ribbons of *Rr*CooT monomers are colored in blue and light blue, while the Ni(II) ion is reported as a green sphere and Met1 and Cys2 from each monomer are depicted as sticks colored accordingly to the atom type. The metal binding site in panels **C** and **F** have been rotated by 90° degrees around the vertical axis with respect to the representations in the other panels. See also Figures S4 and S5 for further details.

binding region is in a similar orientation with respect to the Amide-Cis1 model, but the Ni(II) coordination geometry is strongly distorted (rmsd_ig = 0.509 Å) and the metal ion is less exposed to the solvent. Finally, the Amide-Trans model (Figure 7F) resulted in a metal binding region oriented in a similar arrangement with respect to the Amino-Trans model. The plane defined by the metal ligands is parallel to the dimer's major axis and the Ni(II) ion is exposed to the solvent only on one side. The coordination geometry is only slightly distorted with respect to the ideal geometry (rmsd_ig = 0.121 Å). As in the previous set of amino models, in both Amide-Cis1 and Amide-Cis2 models the side chains of $Met1_A$ and $Met1_B$ are buried inside the protein, while in the case of Amide-Trans model the side chain of Met1 from both monomers lies on the dimer surface. Considering the distortion of the metal binding geometry achieved in both model Amino-Cis2 (Figure 7B) and Amide-Cis2 (Figure 7E), these models were not considered in the following refinement of the structural parameters extracted from the EXAFS data.

EXAFS structural refinement

Theoretical EXAFS signals were thus simulated for structure-optimized square planar NiN_2S_2 clusters considering the Amino-Cis1 (Figure 7A) Amino-Trans (Figure 7C), Amide-Cis1 (Figure 7D) Amide-Trans (Figure 7F) models. For simulations of the EXAFS spectra, a shell of 4.5 Å around the Ni absorber was considered. This approach resulted in 20-atoms clusters that included the backbone atoms of Met1 and Cys2, together with the side chain of Cys2. None of the optimized models showed asymmetric Ni-N distances for the two N donors, as instead suggested by the first-shell EXAFS analysis. Consistently, the corresponding simulated EXAFS spectra (Figure 6C), solid black lines) did not reproduce the experimental oscillations, and further

refinement was needed. Thus, each of the theoretical EXAFS spectra was fitted to the experimental data in the reciprocal space applying the rigid-body-refinement scheme, i.e. allowing first-shell distances and DW factors to vary, while constraining outer shell atoms to move rigidly following the variation in first-shell distances. Any attempt to assign a single Ni-N distance to the two first-shell Ni-N paths resulted in a significant overestimation of the Ni-N Debye-Waller factors ($\sigma^2 > 0.02$ Å^2); therefore, those fits were rejected, and two distinct Ni-N distances were introduced. Upon refinement, the theoretical signal generated from the Amide-Trans model (Figure 7F) provided the best agreement with the experimental data (fit number 3 in Table 1, red curve in Figure 6C), whereas the other three models failed to reproduce the data (either the fit did not converge, or it provided unphysical parameters).

DISCUSSION

In proteins, the most common nickel-coordinating amino acid is histidine while the distribution of cysteine is much less important. [30] However, cysteine is known to be a special case among amino acids because of its unique properties due to its nucleophilicity, its high affinity for metals and its ability to form disulphide bridges. With its tuneable chemical reactivity, this amino acid plays crucial roles as Ni ligands in active sites of redox Ni enzymes, such as CODH, ACS or [NiFe]-hydrogenases to lower the potential of the reducing couple thanks to the high reactivity of its thiol group. Instead, histidines are preferred to coordinate Ni(II) ions in non-redox proteins.[16, 20] However, cysteine-rich coordinating motifs, known to be excellent nickel binders, can be also found in some nickel chaperones, such as HypB [18] or HspA from *H. pylori*. [31] In the latter case, histidines are also present, suggesting a mixed His/Cys nickel-binding pattern. Interestingly, cysteine exhibits extreme patterns of conservation, being either highly conserved or completely degenerated. When cysteines are conserved, the degree of conservation is typically above 90%, highlighting its essential role. Another feature of cysteine is its tendency to clustering with other cysteines, which has been highly favoured during evolution.

The case of *Rr*CooT and its homologues is somehow intriguing: not only this nickel chaperone possesses neither cysteine-rich region nor nearby histidines in the sequence, but also the protein dimerization forms a solvent-exposed nickel-binding site with two cysteine residues via a single cysteine motif. In this way, the homo-dimerization allows the clustering of cysteines from two different peptide chains. Moreover, the exposure of isolated cysteines is associated with a considerable increase in its reactivity, which is generally a drawback for experimental analyses. [20] In *Rr*CooT, the proximity of the two Cys2 leads, upon oxygen exposure, to the rapid formation of a disulphide bridge with the formation of a homogenous covalent dimer, as shown by ESI-MS. While this phenomenon prevents Ni(II) binding, it protects the protein from intermolecular disulphide bridges formation, multimerization and even precipitation. Moreover, as shown by NMR, the phenomenon is fully reversible by addition of TCEP, recovering the ability of *Rr*CooT to bind Ni(II). Since *Rr*CooT is involved in anaerobic metabolism, it is likely to easily bind Ni(II) ions present in its natural environment.

Focusing on the nature of the *Rr*CooT ligands for Ni(II), the present study strongly indicates that this metal ion binds two S and two N from the two proximal Cys2 side chains and backbones, respectively. The arrangement of the dimer, as supported by a combination of experimental and modelling studies, is such that the two cysteine side chains are in *trans* position with respect to the metal ion.

Although amidate groups are unusual biological ligands, [32] Ni(II) is able to induce deprotonation and metal ion coordination of the peptide amide N atoms. [33] Among the Ni(II)-N_2S_2 moieties found in proteins, the redox enzyme NiSOD harbours a Ni(II) ions coordinated by the two thiolates of Cys2 and Cys6, the terminal amine and the amide group of Cys2 in its reduced state [17]. Several NiSOD model peptides and complexes have been synthesized in which the N-donor ligands were varied from the natural mixed amine/amidate environment to a bis-amidate one, leading exclusively to catalytically inactive species. One reason would be that bis-amidate complexes are considered to be more reactive towards O_2.[34] However, the effect of bis-amidate vs mixed amine/amidate environment on the oxygen stability of NiSOD model peptides and NiN_2S_2 complexes is controversial. [35] A bis-amidate coordination has also been observed in the Ala0-NiSOD mutant [23], which possesses an Ala N-terminal extension, resulting in a S $\rightarrow$ Ni LMCT red-shift transition from 380 nm for the wild-type enzyme to 457 nm, this reddish color being similar to the one observed with Ni-*Rr*CooT. In the mutant form, the terminal amine coordination observed in WT-NiSOD is replaced by the amide group of His1, resulting in the abolition of the enzyme activity and an increase in air sensitivity with the appearance of disulphide and S-oxygenated species over two weeks.

In biology, the only example of a Ni(II) centre with a bis-amidate/bis-thiolate environment has been identified in the active site of acetyl-coenzyme A synthase. [36] This enzyme possesses a dinuclear Ni active site, with one distal nickel (Ni_d), coordinated by an unusual Cys-Gly-Cys motif in a square planar geometry involving the thiolates of both cysteines and the amido N atoms of a cysteine and a glycine. The same cysteines also coordinate the proximal nickel (Ni_p), which is the catalytic centre of the enzyme. Ni_d is postulated not to be involved in redox chemistry and to remain in the Ni(II) state. [37] Its role has been proposed either as a supporting ligand to stabilize the proximal nickel in a low-valent redox level [22, 38] or for the generation of an open site on the catalytic metal thanks to its hemilabile ring-opening property. [38-39] These hypotheses arise from the investigations on Ni-N_2S_2 complexes that have been shown to be i) good electron donors and ii) able to bind as mono- or bidentate ligands, a property fundamental to hemilability. [39-40] Among the library of monomeric square planar Ni(II)-N_2S_2 complexes with either amino- or amidato N donors, tetra-anionic amido-thiols favor the reduction of Ni(II) to Ni(I) at highly negative potentials while biologically-relevant potentials would stabilize the Ni(II)/Ni(III) couple. [38] All these examples show that the presence of N donors as well as their nature tune the chemical properties of the metal centre.

It is worth mentioning that CooT likely works in concert with its partners, with the ultimate goal of transferring Ni(II) to CODH. Moreover, the existence of the two distinct metal-binding motifs, namely “Cys2” and “Cys2-His55” raises the question of their physiological role. While the “Cys2” motif in *Rr*CooT allows Ni(II) binding with an affinity in the nanomolar range, *Ch*CooT possessing the predicted “Cys2His55” motif binds Ni(II) in the micromolar range, [19] possibly hinting to distinct functions *in vivo*. In *R. rubrum*, CooT has been experimentally shown to be involved in CODH maturation. Therefore, despite a high affinity for Ni(II), the metal release is required and could occur via the interaction with CooJ, CooC or/and CODH. The solvent exposure of the nickel-binding site in *Rr*CooT makes it possible to consider that the cooperation with its partner(s) would induce a change in coordination and affinity, facilitating Ni(II) release. However, the precise role of *Rr*CooT has not be fully demonstrated and to date, no information is available regarding the role of other CooT homologues.

To conclude, a single cysteine motif for Ni(II) makes *Rr*CooT a unique example among Ni chaperones. The binding of a mononuclear Ni(II) ion with a N_2S_2 environment via a bis-thiolate/bis-amidate coordination is unprecedented and its role remains to be clarified. It is not fully understood how the N_2S_2 ligands contribute to the physiological role of *Rr*CooT.

Experimental Section

The details of protein production and purification, CD, UV-vis and NMR spectroscopies as well as ITC experiments are provided as Supplementary Information.

Molecular Modelling: The Ni(II) bound form of *Rr*CooT was generated using Modeller v9.18, [41] and the structure of apo-*Rr*CooT (PDB id: 5N76) as template. [15] A single Ni(II) ion was included in the model, in agreement with metal content analyses and ITC experiments previous reported. [15] The van der Waals parameters for Ni(II) were derived from the Zn(II) parameters included in the CHARMM22 force field, [32] implemented in the Modeller v9.18 package, by applying a scale factor (1.12) calculated on the basis of the ionic radius of the two divalent ions. The best structure among the 100 generated models was selected on the basis of the lowest value of the DOPE score included in Modeller v9.18, [42] and the analysis performed with PROCHECK. [43] A loop optimization routine was used to refine the metal binding region. In all modelling calculations, constraints were imposed using a Gaussian-shaped energy potential for distances, angles, and dihedrals in order to correctly position the Ni(II) ions with respect to the tested list of ligated atoms (Table S4). The best model was selected on the basis of the lowest value of the DOPE score. The molecular graphics, together with analysis of the Ni(II) sites, were performed using the UCSF Chimera package. [44]

X-ray Absorption Spectroscopy**:** Ni K-edge X-ray absorption spectroscopy (XAS) was performed at the beamline CRG-FAME-BM30B of the European Synchrotron Radiation Facility (ESRF, Grenoble, France).[45] Apo-*Rr*CooT-WT was concentrated to 1.5 mM and incubated with 0.9 molar eq. of $NiSO_4$ for 10 minutes before addition of 10 % glycerol as cryoprotectant. Drops of the solution (~50 µL) were deposited on the Ø5mm holes of the sample holder equipped with kapton windows, immediately frozen in liquid nitrogen, then transferred into the liquid He-cryostat and measured at 15 K in order to limit radiation damages. Depending on the Ni concentration, 5 to 10 spectra were acquired for the same sample, then merged. The position of the beam (size: 205x120 µm², FWHM) was changed for each acquisition in order to limit the effects of X-ray irradiation. The Ni K-edge energy region was scanned in the 8100-9300 eV range with a liquid nitrogen-cooled Si(220) monochromator. The photon energy was calibrated using a metallic Ni foil, by defining the first inflection point of its absorption spectrum at 8333.0 eV. X-ray absorption spectra were recorded in fluorescence mode with a 30-elements Ge solid-state detector (Canberra).
XAS data reduction and normalization was performed with standard methods using the Athena software. [46] Peak fitting in the XANES region was performed with the Fityk program, using a Levenberg-Marquardt minimization algorithm. [47] A detailed description of the data analysis protocol is reported in the SI.

Acknowledgements

This work was supported by “the ITERLIS PhD program, CEA Life sciences” for MA’s PhD funding, the “FUNBIOCO” project (IDEX-UGA, Initiatives de Recherche stratégiques) and the “COSYNBIO” project (Projets exploratoires, Cellule energie-CNRS). This work has been partially supported by Labex ARCANE and CBH-EUR-GS (ANR-17-EURE-0003). The research leading to these results has received funding from the networking support from the COST Action FeSBioNet (Contract CA15133). This work used the platforms of the Grenoble Instruct-ERIC Center (ISBG: UMS3518CNRS-CEA-UGA-EMBL) with support from FRISBI (ANR-10-INBS-05-02) and GRAL (ANR-10-LABX-49-01) within the Grenoble Partnership for Structural Biology (PSB). The authors gratefully acknowledge the European Synchrotron Radiation Facility program committee (Grenoble, France) for provision of beamtime (LS-2473) and the CRG-FAME for the In-house-Research beamtime (IH-LS-2796) and support of their staff. The authors acknowledge the support and the use of resources of Instruct-ERIC. This work was supported by the Department of Pharmacy and Bio- technology of the University of Bologna (SC, BZ, FM). The NMR experiments were partially obtained in the frames of access to NMR infrastructure by EuroBioNMR EEIG (http://www.eurobionmr.eu/). The Center for Magnetic Resonance of the University of Florence (CERM) provided access to the high-field NMR spectrometers. Fabio Calogiuri and Massimo Lucci are acknowledged for spectral data collection.

Keywords: Carbon monoxide dehydrogenase maturation • Ni chaperone protein • Ni(II)N_2S_2 coordination • CooT • Nickel-binding cysteine

References

[1] Y. Sheng, I. A. Abreu, D. E. Cabelli, M. J. Maroney, A.-F. Miller, M. Teixeira, J. S. Valentine, *Chem Rev* **2014**, *114*, 3854-3918.
[2] M. J. Maroney, S. Ciurli, *Chem. Rev.* **2014**, *114*, 4206-4228.
[3] P. N. Evans, J. A. Boyd, A. O. Leu, B. J. Woodcroft, D. H. Parks, P. Hugenholtz, G. W. Tyson, *Nature Reviews Microbiology* **2019**, *17*, 219-232.
[4] M. Can, F. A. Armstrong, S. W. Ragsdale, *Chem Rev* **2014**, *114*, 4149-4174.
[5] M. Alfano, C. Cavazza, *Sustainable Energy & Fuels* **2018**, *2*, 1653-1670.
[6] R. L. Kerby, P. W. Ludden, G. P. Roberts, *Journal of bacteriology* **1995**, *177*, 2241-2244.
[7] J. D. Fox, R. L. Kerby, G. P. Roberts, P. W. Ludden, *J. Bacteriol.* **1996**, *178*, 1515-1524.
[8] C. L. Drennan, J. Heo, M. D. Sintchak, E. Schreiter, P. W. Ludden, *Proceedings of the National Academy of Sciences* **2001**, *98*, 11973-11978.
[9] S. W. Singer, M. B. Hirst, P. W. Ludden, *Biochim Biophys Acta* **2006**, *1757*, 1582-1591.
[10] D. Bonam, M. C. McKenna, P. J. Stephens, P. W. Ludden, *Proceedings of the National Academy of Sciences* **1988**, *85*, 31-35.
[11] Y. Li, D. B. Zamble, *Chem Rev* **2009**, *109*, 4617-4643.
[12] R. L. Kerby, P. W. Ludden, G. P. Roberts, *J. Bacteriol.* **1997**, *179*, 2259-2266.
[13] W. B. Jeon, J. Cheng, P. W. Ludden, *J Biol Chem* **2001**, *276*, 38602-38609.
[14] M. Alfano, J. Pérard, P. Carpentier, C. Basset, B. Zambelli, J. Timm, S. Crouzy, S. Ciurli, C. Cavazza, *J. Biol. Chem.* **2019**.
[15] J. Timm, C. Brochier-Armanet, J. Perard, B. Zambelli, S. Ollagnier-de-Choudens, S. Ciurli, C. Cavazza, *Metallomics* **2017**, *9*, 575-583.
[16] S. M. Marino, V. N. Gladyshev, *Journal of molecular biology* **2010**, *404*, 902-916.
[17] D. P. Barondeau, C. J. Kassmann, C. K. Bruns, J. A. Tainer, E. D. Getzoff, *Biochemistry* **2004**, *43*, 8038−8047.
[18] M. R. Leach, S. Sandal, H. Sun, D. B. Zamble, *Biochemistry* **2005**, *44*, 12229-12238.

[19] M. Alfano, J. Perard, R. Miras, P. Catty, C. Cavazza, *J Biol Inorg Chem* **2018**, *23*, 809-817.
[20] L. B. Poole, *Free Radical Biology and Medicine* **2015**, *80*, 148-157.
[21] J. Jeong, Y. Jung, S. Na, J. Jeong, E. Lee, M.-S. Kim, S. Choi, D.-H. Shin, E. Paek, H.-Y. Lee, K.-J. Lee, *Molecular & Cellular Proteomics* **2011**, *10*.
[22] R. Krishnan, C. G. Riordan, *Journal of the American Chemical Society* **2004**, *126*, 4484-4485.
[23] H.-T. Huang, S. Dillon, K. C. Ryan, J. O. Campecino, O. E. Watkins, D. E. Cabelli, T. C. Brunold, M. J. Maroney, *Inorg. Chem.* **2018**, *57*, 12521-12535.
[24] N. Lihi, G. Csire, B. Szakács, N. V. May, K. Várnagy, I. Sóvágó, I. Fábián, *Inorganic Chemistry* **2019**, *58*, 1414-1424.
[25] Y. Shen, F. Delaglio, G. Cornilescu, A. Bax, *J Biomol NMR* **2009**, *44*, 213-223.
[26] L. Wang, H. R. Eghbalnia, A. Bahrami, J. L. Markley, *J Biomol NMR* **2005**, *32*, 13-22.
[27] G. J. Colpas, M. J. Maroney, C. Bagyinka, M. Kumar, W. S. Willis, S. L. Suib, N. Baidya, P. K. Mascharak, *Inorg. Chem.* **1991**, *30*, 920-928.
[28] a Y. Oudart, V. Artero, J. Pécaut, C. Lebrun, M. Fontecave, *European Journal of Inorganic Chemistry* **2007**, *2007*, 2613-2626; b Johanna A. W. Verhagen, M. Lutz, Anthony L. Spek, E. Bouwman, *European Journal of Inorganic Chemistry* **2003**, *2003*, 3968-3974; c H. J. Kruger, G. Peng, R. H. Holm, *Inorganic Chemistry* **1991**, *30*, 734-742.
[29] V. Martin-Diaconescu, M. Bellucci, F. Musiani, S. Ciurli, M. J. Maroney, *J Biol Inorg Chem* **2012**, *17*, 353-361.
[30] R. J. Sudan, J. L. Kumari, C. Sudandiradoss, *PLoS One* **2015**, *10*, e0126787.
[31] K. Schauer, C. Muller, M. Carrière, A. Labigne, C. Cavazza, H. De Reuse, *Journal of bacteriology* **2010**, *192*, 1231.
[32] A. MacKerell, D. Bashford, M. Bellot, R. Dunbrack, J. Evanseck, M. Field, *J. Phys. Chem. B* **1998**, *102*, 3586-3616.
[33] D. Zamble, M. Rowińska-Żyrek, H. Kozlowski, in *Metallobiology, Vol. 10* (Ed.: C. D. Garner), Royal Society of Chemistry, Cambridge (UK), **2017**.
[34] a V. Mathrubootham, J. Thomas, R. Staples, J. McCraken, J. Shearer, E. L. Hegg, *Inorganic Chemistry* **2010**, *49*, 5393-5406; b K. P. Neupane, J. Shearer, *Inorganic Chemistry* **2006**, *45*, 10552-10566.
[35] D. Tietze, J. Sartorius, B. Koley Seth, K. Herr, P. Heimer, D. Imhof, D. Mollenhauer, G. Buntkowsky, *Scientific reports* **2017**, *7*, 17194-17194.
[36] C. Darnault, A. Volbeda, E. J. Kim, P. Legrand, X. Vernède, P. A. Lindahl, J. C. Fontecilla-Camps, *Nature Structural & Molecular Biology* **2003**, *10*, 271-279.
[37] E. L. Maynard, C. Sewell, P. A. Lindahl, *Journal of the American Chemical Society* **2001**, *123*, 4697-4703.
[38] M. L. Golden, M. V. Rampersad, J. H. Reibenspies, M. Y. Darensbourg, *Chemical Communications* **2003**, 1824-1825.
[39] K. N. Green, S. P. Jeffery, J. H. Reibenspies, M. Y. Darensbourg, *Journal of the American Chemical Society* **2006**, *128*, 6493-6498.
[40] M. L. Golden, C. M. Whaley, M. V. Rampersad, J. H. Reibenspies, R. D. Hancock, M. Y. Darensbourg, *Inorganic Chemistry* **2005**, *44*, 875-883.
[41] M. A. Marti-Renom, A. C. Stuart, A. Fiser, R. Sanchez, F. Melo, A. Sali, *Annu. Rev. Biophys. Biomol. Struct.* **2000**, *29*, 291-325.
[42] M.-y. Shen, A. Sali, *Protein Science* **2006**, *15*, 2507-2524.
[43] R. A. Laskowski, M. W. MacArthur, D. S. Moss, J. M. Thornton, *J. Appl. Crystallograph.* **1993**, *26*, 283-291.
[44] E. F. Pettersen, T. D. Goddard, C. C. Huang, G. S. Couch, D. M. Greenblatt, E. C. Meng, T. E. Ferrin, *J. Comput. Chem.* **2004**, *25*, 1605-1612.
[45] O. Proux, X. Biquard, E. Lahera, J. J. Menthonnex, A. Prat, O. Ulrich, Y. Soldo, P. Trvisson, G. Kapoujyan, G. Perroux, P. Taunier, D. Grand, P. Jeantet, M. Deleglise, J. P. Roux, J. L. Hazemann, *Physica Scripta* **2005**, 970.
[46] B. Ravel, M. Newville, *J. Synchrotron Radiat.* **2005**, *12*, 537-541.
[47] M. Wojdyr, *J. Appl. Cryst.* **2010**, *43*, 1126-1128.

Entry for the Table of Contents (Please choose one layout)

Layout 1:

RESEARCH ARTICLE

Text for Table of Contents

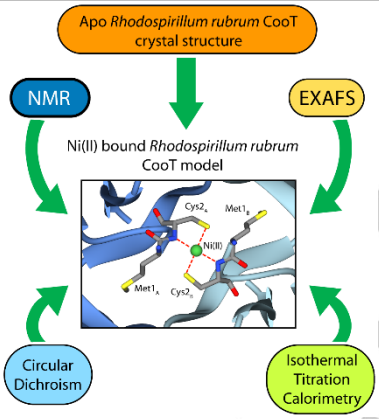

*Author(s), Corresponding Author(s)**

Page No. – Page No.

Title